Research Article

Preparation of hydroxyapatite ceramic through centrifugal casting process using ultra-fine spherical particles as precursor and its decomposition at high temperatures

Yanjie ZHANG [a,b], Jinjun LU [a,*], Shengrong YANG [a]

[a] *State Key Laboratory of Solid Lubrication, Lanzhou Institute of Chemical Physics,*
Chinese Academy of Sciences, Lanzhou 730000, China

[b] *Graduate School of the Chinese Academy of Sciences, Beijing 100039, China*

Abstract: Ultra-fine hydroxyapatite (HAp) powder with a diameter of about 10 nm was used as precursor for preparation of HAp ceramic. The precursor hydroxyapatite was single phase and highly crystallized without any additional thermal treatment. Highly densified HAp ceramic was fabricated through centrifugal infiltration casting (CIC), followed by pressureless sintering. The relative densities of compacts prepared at 1100°C and 1200°C were 77.8% and 94.1%, respectively. SEM micrographs of HAp ceramic sintered at 1100°C showed a porous microstructure with a grain size of 1 μm. HAp ceramic fabricated at 1200°C revealed a dense microstructure with nano-sized spherical α-TCP distributed at grain boundaries and triple points. The mechanism of decomposition from HAp to α-TCP at 1200°C was discussed on the basis of SEM, XRD and FTIR results.

Key words: hydroxyapatite; bioceramics; Centrifugal Infiltration Casting; pressureless sintering

1 Introduction

Hydroxyapatite (HAp) is a bioactive ceramic with a crystal structure similar to the native bone and teeth minerals. Ceramic hydroxyapatites are widely used in biomedical applications because of their high biocompatibility and forming bonds with living tissues [1,2]. Despite its high bioactivity, HAp is limited in applications due to the poor mechanical strength.

Hence highly densified HAp compact has been investigated for possible application as load-bearing implants. High-density ceramics of HAp are currently prepared by pressure-assisted sintering [3-5]. The morphology and size of HAp powder influence the quality of the ceramic material. There are several different synthesis methods used to generate HAp such as chemical precipitation [6], hydrothermal [7-9], sol-gel [5,10,11], and mechanochemical methods [12,13]. The chemical precipitation approach has been chosen because it will likely generate the desired stoichiometry, crystalline phase and grain size at low temperature.

Green pellets of HAp were obtained by isostatic

---

* Corresponding author.
E-mail: jjlu@lzb.ac.cn
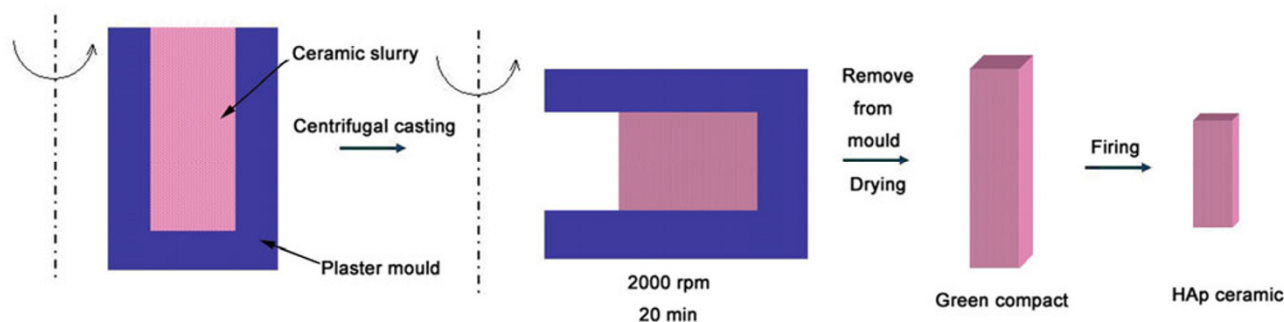Tel: +86-931-4968198; Fax: +86-931- 4968198.

Fig. 1   Schematic illustration of centrifugal casting process

pressing and followed by pressure-assisted sintering process. The HAp ceramics prepared by this process exhibited a dense microstructure and excellent bending strength. It was also reported that the relative density of pressureless sintered HAp could not be higher than 70 % of the theoretical density [3]. However, the drawback of the pressure-assisted sintering process lies in the difficulty in preparing HAp components with complex shapes.

Centrifugal infiltration casting (CIC) is derived from centrifugal casting, which is also a powerful colloidal processing for massive production of ceramic parts with complex shapes. The two molding processes are different in removing solvent from slurries. In the centrifugal casting process, the supernatant is poured off from steel moulds after centrifugation, which will cause possible mass and phase segregation during the consolidation stage [14,15]. While in the centrifugal infiltration casting process, the solvent is equably infiltrated in the plaster moulds under a high-speed centrifugation. Therefore the centrifugal infiltration casting process enables to obtain green compacts with a uniform microstructure.

The decomposition of HAp results in changes of mechanical and physicochemical properties of the final materials. Thus, the thermal stability of hydroxyapatite has been widely investigated in the past years, for example, the thermal stability of HAp during hot pressing and pressureless sintering by FTIR and XRD analysis [16] and the properties of porous hydroxyapatite bioceramic produced by the annealing of bovine bone [17].

In the present study, highly densified HAp ceramics were prepared by CIC process and pressureless sintering using ultra-fine HAp particles as precursor. The decomposition mechanism of HAp ceramic was also studied by SEM, XRD and FTIR analysis.

2 Experimental procedure

2.1 Synthesis of ultra-fine HAp powders

Calcium nitrate ($Ca(NO_3)_2 \cdot 4H_2O$), diammonium hydrogen phosphate (($NH_4)_2HPO_4$) and ammonium hydroxide (NH_4OH) (all analytical grade) were used as reactants. To precipitate HAp, 0.5 M ($NH_4)_2HPO_4$ in deionized water was added to 0.5 M ($Ca(NO_3)_2 \cdot 4H_2O$) in ethanol with vigorous stirring. The pH of these precursor solutions was adjusted to 10~11 by the addition of concentrated NH_4OH. After reaction for 1 h at 40°C, the product was kept inside an oven at 30°C overnight. Then it was washed three times by water and filtered by centrifuging.

2.2 Preparation of HAp ceramics

Slurries with 14% solid loading were obtained by the filtered ultra-fine HAp powders with 20 ml ethanol through ultrasonic treatment, then consolidated by a high-speed centrifugal machine at 2000 rpm for 20 min in plaster moulds. After centrifugation, green compacts ($42 \times 9 \times 6$ mm^3) were obtained and dried at room temperature in open air (relative humidity of 40%-50%) for five days. The whole process was shown in Fig. 1. Finally, those green compacts were sintered for 4 h in air at 1100°C and 1200°C, respectively.

2.3 Characterization

The density of the sintered sample was measured by the Archimedes method. The relative densities of HAp ceramics were obtained using the measured densities over their theoretical density (3.16 g/cm^3). Phase compositions of the ultra-fine HAp powders and the sintered sample were examined by X-ray diffraction (XRD) with Cu Kα radiation (λ=1.5418 Å). The diffractometer (X'Pert PRO, Philips) was operated at

40 kV and 30 mA at a 2θ range of 20º-70º employing a step size of 0.0170 and a 29.8450 s exposure. The products were also characterized by Fourier transform-infrared spectroscopy (FT-IR, IFS 66V/S FTIR, Bruker) in the range of 4000 cm^{-1}-400 cm^{-1}. The elemental analysis was conducted by ICP-AES (IRIS Advantage ER/S). The morphology and grain size of the synthesized powders were observed by transmission electron microscopy (TEM, H-600, Hitachi). Surface morphology was observed by scanning electron microscopy (SEM, JSM5600LV, JEOL) on the surface and cross section of the sintered sample.
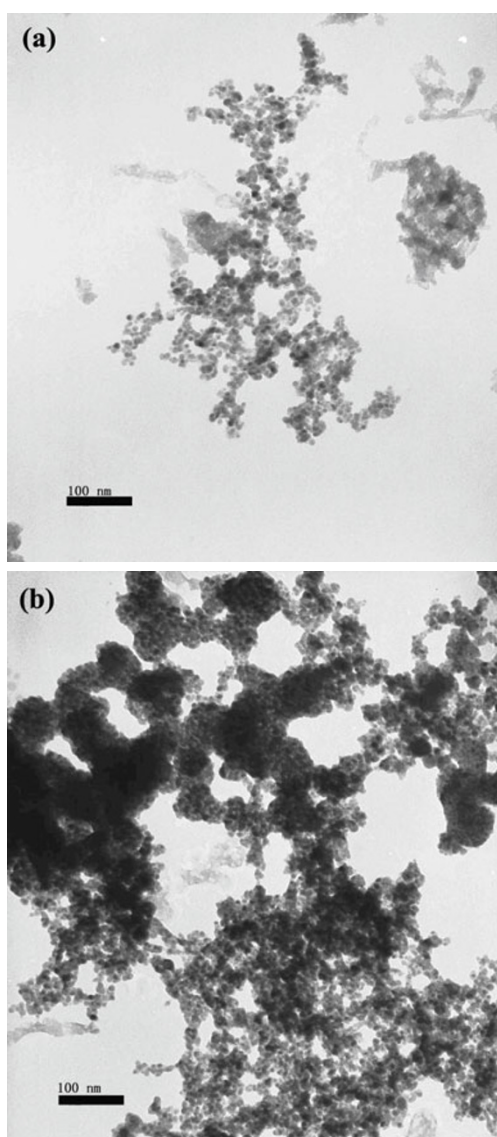

Fig. 2   TEM micrographs of ultra-fine HAp particles: (a) ultra-fine crystal and (b) spherical aggregation self-aligned by ultra-fine particles

3 Results and discussion

3.1 Ultra-fine HAp particles

The ultra-fine HAp particles were obtained without additional thermal treatment. The TEM micrograph (Fig. 2a) shows the ball-like structure of as-synthesized ~10 nm HAp crystal. Because of the high surface energy, ultra-fine particles are easily self-aligned in spherical aggregates approximately 100 nm in diameter, as shown in Fig. 2b. Therefore, the thermal treatment facilitates the aggregation and finally results in the growth of HAP from ultra-fine crystal to large particle. The raw HAp powder is calcium deficient and carbonate free (See the later FTIR spectrum) with the Ca/P ratio of 1.55.

3.2 Shrinkage of green compacts

Although the solvent in the suspension is partially removed during the CIC process, the green compact after CIC process is still solvent-containing. The compact tends to shrink via evaporation of residual solvent during drying. The relationship between linear shrinkage (Ls) and drying time (Fig. 3) shows that shrinkage mainly occurs within 30 h, often which remains constant at about 30%.

3.3 Relative density and microstructure of HAp ceramics

A SEM observation of the fractured surface of 77.8% dense HAp ceramic sintered at 1100 ℃ is shown in Fig. 4. The average grain size of HAp markedly increases from ~10 nm of the precursor to ~1 μm at 1100 ℃
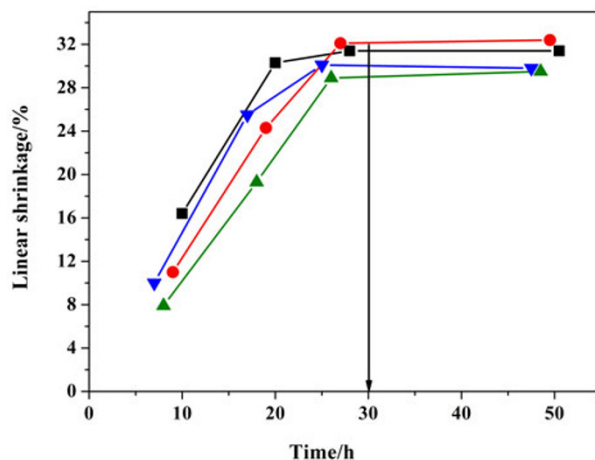

Fig. 3   Relationship between linear shrinkage and drying time of green compacts (four samples)
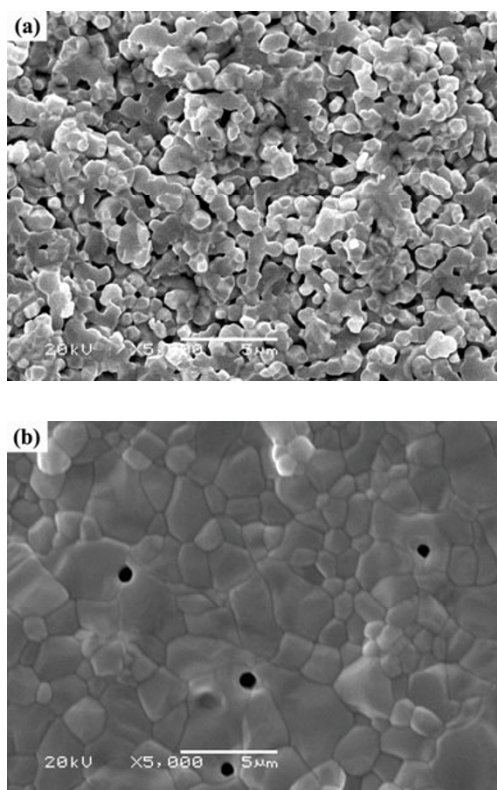
Fig. 4   SEM micrographs of cross-sectionals: (a) HAp ceramic sintered at 1100 ℃, (b) HAp ceramic sintered at 1200 ℃
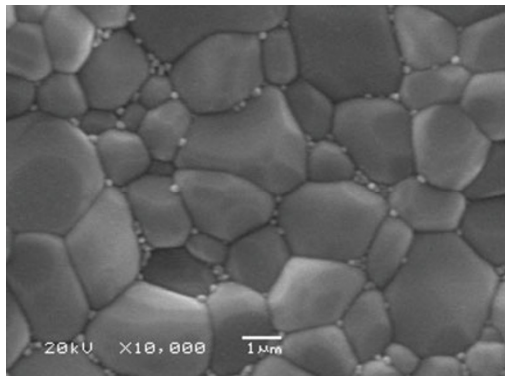

Fig. 5   SEM micrographs of the outermost surface for HAp ceramics sintered at 1200 ℃

(Fig. 4a) and several micrometers at 1200 ℃℃ (Fig. 4b). The 94.1% dense sample sintered at 1200 ℃ shows nearly equiaxed uniform microstructure except for a few spherical pores on the boundary of the HAp grains.

SEM micrograph of Fig. 5 reveals different microstructures on the outermost surface and the fractured surface of HAp ceramic sintered at 1200 ℃ consisting of some small spherical particles (12-13 nm in diameter) at grain boundaries and triple points.

3.4 Decomposition mechanism of HAp ceramic

It can be observed that ultra-fine HAp precursor is single phase and highly crystallized (Fig. 6a) and all peaks corresponded with HAp based on the standard XRD pattern of HAp (JCPDS card no. 09-432). XRD analysis of sample sintered at 1100 ℃ and 1200 ℃ reveals the presence of a small amount of α-TCP phase (α-tricalcium phosphate marked with ♦ in Figs. 6b and c), which derived from decomposition of HAp ceramic at 1200 ℃. Therefore, those small particles at grain boundaries and triple points on the outermost surface of HAp ceramic in Fig. 5 are the decomposition product (α-TCP) of HAp because of high reaction activity on grain boundary. The decomposition of HAp begins from the outside of the ceramic body at 1200 ℃ and the decomposition product appears only on the surface of the ceramic body.

Fig. 7 shows the FT-IR spectra of ultra-fine HAp powder and the samples sintered at 1100 ℃ and 1200 ℃. In Fig. 7a, the hydroxyl stretching bands and bending bands of HAp are assigned respectively at 3569 cm^{-1} and 632 cm^{-1}, while the broad band at 3414 cm^{-1} corresponds to the absorbed water. The adsorptions at 1095, 1035, 962, 603, and 566 cm^{-1} are attributed to PO_4^{3-} ions (v_1-962 cm^{-1}, v_3-1035 cm^{-1} and 1095 cm^{-1}, v_4-566 cm^{-1} and 603 cm^{-1}) [19,20]. The
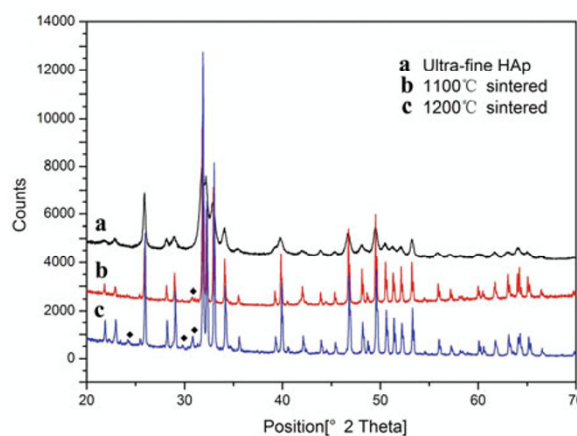

Fig. 6   XRD patterns of (a) ultra-fine HAp powder, (b) and (c) HAp ceramics sintered at 1100°C and 1200°C for 4 h, respectively. ♦ peaks correspond to α-tricalcium phosphate (JCPDS card no. 09-348), all the other peaks correspond to hydroxyapatite based on the standard XRD pattern card of HAp (JCPDS card no. 09-432)
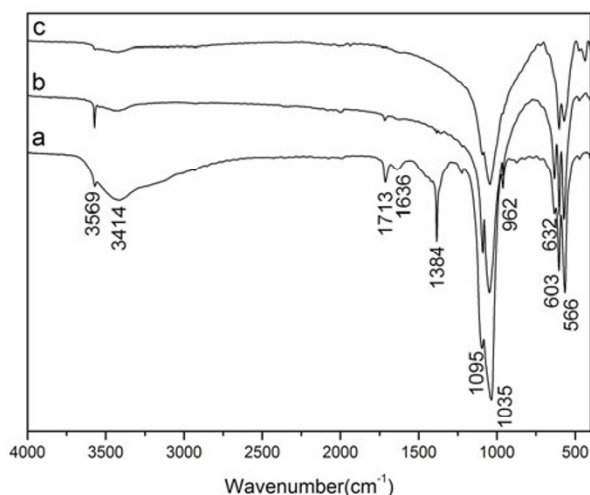
Fig. 7 FT-IR spectra of HAp samples: (a) ultra-fine HAp powder; (b) and (c) HAp ceramic sintered at 1100 ℃ and 1200 ℃, respectively

broad band at 3211 cm^{-1} and the adsorption at 1384 cm^{-1} are originated from NH$_4^+$ on the surface of HAp crystal, which will decompose at high temperature. In Fig. 7, the intense band of hydroxyl group blueshift from 3569 cm^{-1} to 3572 cm^{-1}, along with increase of intensity. Fig. 7c shows that the bands at 3572 cm^{-1} and 632 cm^{-1} disappear completely at a sample temperature of 1200 ℃, which indicates the dehydration of OH group at 1200 ℃.

The decomposition mechanism is proposed on the basis of above experimental results. The decomposition of HAp begins from dehydration of OH group at 1200 ℃, which results in the formation of intermediate (oxyapatite). The dehydration occurs according to the following reactions [21,22]:

$$2OH \rightarrow O + H_2O(g) \qquad (1)$$

$$Ca_{10}(PO_4)_6(OH)_2 \rightarrow Ca_{10}(PO_4)_6O\bullet + H_2O(g) \qquad (2)$$
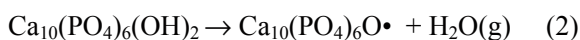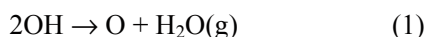
The □ means a non-charged vacancy and the hydroxyl-deficient product Ca$_{10}$(PO$_4$)$_6$O •□ is known as oxyapatite. Further decomposition of HAp will result in the formation of tricalcium phosphate (TCP phase).

In this study, high temperature (1200 ℃) leads to decomposition of HAp ceramic to α-TCP (Figs. 6b and 6c). Because of high activity on the verges of HAp grains, the decomposition firstly begins from the crystal verge. Therefore, the decomposed product (small spherical particle) was usually found on the grain

boundary at the surface of sintered body (Figs. 5a and 5b). However, it should be noted that the transformation of HAp to α-TCP phase is rather limited in this work.

4 Conclusion

Through CIC process and pressureless sintering, highly densified HAp ceramics is prepared from ultra-fine spherical particles precursor. Sintering temperature is vital for the densification and grain sizes of HAp ceramics. At 1200 ℃, nearly equiaxed uniform microstructure could be obtained. However, high temperature simultaneously results in the formation of larger grains and decomposition of HAp crystal.

References

[1] Afshar A, Ghorbani M, Ehsani N, *et al*. Some important factors in the wet precipitation process of hydroxyapatite. *Mater design* 2003, **24**: 197-202.

[2] Riman RE, Suchaned WL, Byrappa K, *et al*. Solution synthesis of hydroxyapatite designer particulates. *Solid State Ionics* 2002, **151**: 393-402.

[3] Ahn ES, Gleason NJ, Nakahira A, *et al*. Nanostructure processing of hydroxyapatite-based bioceramics. *Nano Lett* 2001, **1**: 149-153.

[4] Rodriguez-Lorenzo LM, Vallet-Regi M, Ferreira JMF. Fabrication of hydroxyapatite bodies by uniaxial pressing from a precipitated powder. *Biomater* 2001, **22**: 583-588.

[5] Han YC, Li SP, Wang XY, *et al*. Synthesis and sintering of nanocrystalline hydroxyapatite powders

by citric acid sol-gel combustion method. *Mater Res Bull* 2004, **39**: 25-32.

[6] Kumar R, Prakash KH, Cheang P, *et al*. Temperature driven morphological changes of chemically precipitated hydroxyapatite nanoparticles. *Langm* 2004, **20**: 5196-5200.

[7] Kim HW, Koh YH, Li LH, *et al*. Hydroxyapatite coating on titanium substrate with titania buffer layer processed by sol-gel method. *Biomat* 2004, **25**: 2533-2538.

[8] Liu HS, Chin TS, Lai LS, *et al*. Hydroxyapatite synthesized by a simplified hydrothermal method. *Ceram Int* 1997, **23**: 19-25.

[9] Ioku K, Yamauchi S, Fujimori H, *et al*. Hydrothermal preparation of fibrous apatite and apatite sheet. *Solid State Ion* 2002, **151**: 147-150.

[10] Liu DM, Yang QZ, Troczynski T. Water-based sol-gel synthesis of hydroxyapatite: process development. *Biomat* 2002, **23**: 691-698.

[11] Kim TS, Kumta PN. Sol-gel synthesis and characterization of nanostructured hydroxyapatite powder. *Mater Sci Eng B* 2004, **111**: 232-236.

[12] Yeong KCB, Wang J, Ng SC. Mechanochemical synthesis of nanocrystalline hydroxyapatite from CaO and $CaHPO_4$. *Biomat* 2001, **22**: 2705-2712.

[13] Mochales C, Briak-Benabdeslam HE, Ginebra MP, *et al*. Dry mechanochemical synthesis of hydroxyapatites from DCPD and CaO: Influence of instrumental parameters on the reaction kinetics. *Biomat* 2004, **25**: 1151-1158.

[14] Rao PG, Iwasa M, Tanaka T, *et al*. Centrifugal casting of Al_2O_3-15wt.%ZrO_2 ceramic composites. *Ceram inter* 2003, **29**: 209-212.

[15] Gao GW, Wang CY. Modeling the solidification of functionally graded materials by centrifugal casting. *Mater Sci Eng A* 2000, **292**: 207-215.

[16] Rapacz-Kmita A, Paluszkiewicz C, Ślósarczyk A, *et al*. FTIR and XRD investigations on the thermal stability of hydroxyapatite during hot pressing and pressureless sintering processes. *J Mol Struct* 2005, **744-747**: 653-656.

[17] Ooi CY, Hamdi M, Ramesh S. Properties of hydroxyapatite produced by annealing of bovine bone. *Ceram Inter* 2007, **33**: 1171-1177.

[18] He ZM, Ma J, Wang C. Constitutive modeling of the densification and the grain growth of hydroxyapatite ceramics. *Biomater* 2005, **26**: 1613-1621.

[19] Carmona P, Garcia-Ramos JV. Polarizable proton-transfer hydrogen bonds between phosphate and organic acids. *J Chem Soc Farad Trans 2* 1985, **81**: 929-935.

[20] Gonzalez-McQuire R, Chane-Ching JY, Vignaud E, *et al*. Synthesis and characterization of amino acid-functionalized hydroxyapatite nanorods. *J Mater Chem* 2004, **14**: 2277-2281.

[21] Liao CJ, Lin FH, Chen KS, *et al*. Thermal decomposition and reconstitution of hydroxyapatite in air atmosphere. *Biomater* 1999, **20**: 1807-1813.

[22] Muralithran G, Ramesh S. The effects of sintering temperature on the properties of hydroxyapatite. *Ceram Inter* 2000, **26**: 221-230.